Available online at www.sciencedirect.com
SCIENCE DIRECT®
Comput. Methods Appl. Mech. Engrg. 195 (2006) 6626–6645
Computer methods in applied mechanics and engineering
www.elsevier.com/locate/cma

Adaptive remeshing based on a posteriori error estimation for forging simulation

Ramzy Boussetta, Thierry Coupez, Lionel Fourment *

CEMEF, École Nationale Supérieure des Mines de Paris, UMR CNRS 7635, BP 207, 06 904 Sophia Antipolis, France

Received 21 February 2005; received in revised form 12 June 2005; accepted 18 June 2005

Abstract

This paper presents a fully automatic 3D adaptive remeshing procedure and its application to non-steady metal forming simulation. Remeshing, here, is considered as the improvement of an existing mesh rather than a complete rebuilding process. The mesh optimization technique is described. It is based on the combination of local improvement of the neighbourhood of nodes and edges. The surface and the volume remeshing are coupled by using a layer of virtual boundary elements. The mesh adaptation is performed by the optimization of the shape factor. The mesh size map enforcement is accounted for working in a locally transformed space. The size map is provided by a Zienkiewicz–Zhu type error estimator. Its accuracy is evaluated in the frame of a velocity/pressure formulation, viscoplastic constitutive equation and 3D linear tetrahedral elements, by numerical experiments. The adaptive remeshing procedure is applied to non-steady forging. Several complex 3D examples show the reliability of the proposed approach to automatically produce optimal meshes at a prescribed computational cost.
© 2005 Published by Elsevier B.V.

Keywords: Meshing; Adaptive remeshing; Error estimation; Forging

1. Introduction: Large deformation and adaptive remeshing

Unstructured mesh generation is a general solution for the construction of a mesh in complex geometries. In a certain number of domains as in forming process simulation, the industrial geometries are really complex. The meshing technique used in this work was developed to solve the remeshing stage in large deformations [1,2]. In such cases, the mesh deforms with the material domain (Lagrangian approach) and thus it degenerates rapidly. In fact, this meshing method is a complete solution in terms of adaptive meshing (including parallel remeshing [3]). Several examples of applications in material forming processes can be found in [4,5]. Although it is based on local improvement mechanism, it is really a mesh generation method which is clearly different from any other well established meshing tool: Delaunay, frontal or octree. The algorithm exploits the possibility to operate on the mesh topologies without considering any geometric constraint. A simple local process is used to derive from mesh to mesh. The node creation and deletion are implicitly contained in the method and the modification of the surface mesh and the volume mesh are strongly coupled. The technique is perfectly suited for forging simulation since it provides a way to repair (elements degeneracy due to the Lagrangian approach) as well as to adapt the mesh to the calculated solution.

A mesh can be adapted dynamically by deriving a new mesh from the old mesh with respect to a mesh size map. A posteriori estimation of the finite element discretization error allows computing an optimal map, which minimizes the mesh

* Corresponding author. Tel.: +33 4 93 95 75 95; fax: +33 4 92 38 97 52.
E-mail addresses: ramzy.boussetta@ensmp.fr (R. Boussetta), thierry.coupez@ensmp.fr, thierry.coupez@cemef.cma.fr (T. Coupez), lionel.fourment@ensmp.fr (L. Fourment).

0045-7825/$ - see front matter © 2005 Published by Elsevier B.V.
doi:10.1016/j.cma.2005.06.029

size for a prescribed accuracy. Many advances have been made in the development of reliable error estimators during the last years. They can be classified into three families: the residual type error estimators, firstly introduced by Babuška and Rheinboldt [6], the estimators based on the error in constitutive relation, developed by Ladevèze et al. [7] and the Zieniewicz–Zhu's (Z^2) [8] type error estimators. In this work, the Z^2 is followed as it is now widely used in many industrial codes due to its efficiency and reliability in estimating errors, as well as for its simplicity of implementation. It is based on the construction of a recovered stress tensor field, $\tilde{\sigma}_h$, more accurate than the finite element solution, σ_h. Initially, $\tilde{\sigma}_h$ was obtained by a variety of projection techniques, such as least square smoothing or simple nodal averaging of adjacent elements values [9]. The approach has been significantly improved by using the superconvergence properties of the finite element solution at some points, and by recovering an enhanced solution inside a local finite element patch. The so-called called superconvergent patch recovery (SPR) technique [10] have been used in a slightly different way by other authors [11,12] who preferred the Liszka–Orkisz local finite difference method [13] to compute the recovered solution from nodal [12] or Gauss integration points [11]. The present study utilizes the Z^2-SPR error estimator in its almost standard form.

The solvers based on tetrahedral meshes are now well established and more particularly finite element method works well both in the context of solid and fluid mechanics. We will focus on a 3D solver developed from a mixed finite element method based on the MINI element (P1+/P1). This solver can be used both in metal forming applications and polymer forming applications. That means that it is usable for small and large deformation of incompressible material and also for incompressible flow of hot polymer and finally to casting. This solver ranges from solid mechanics to fluid mechanics. Moreover, the use of a first order stable tetrahedra (the mini element), allows to have unstructured meshes and iterative solvers [14].

2. Mesh topology optimization

2.1. Mesh topology

The mesh optimization technique used in this paper is based on a simple local mechanism applying on mesh topologies. For that purpose let us introduce notations allowing to introduce precisely the mesh topology. A mesh is determined by a set of coordinates (the mesh node coordinates) and by a set of elements, each element being completely defined by the node numbers of its vertices. The mesh connectivity by means of the element node relations will be called the mesh topology. It can be described independently from any mesh node coordinate.

Let $N \subset \mathbb{N}$ be a finite set of nodes simply reduced to a set of numbers. Let $P_D(N)$ be the set of parts of N which are composed of exactly D different nodes. $\mathscr{T}$, a mesh topology, is a set of elements, $\mathscr{T} \subset P_D(N)$, having the properties described hereafter. The nodes of $\mathscr{T}$ are the subsets of nodes used by $\mathscr{T}$:

$$N(\mathscr{T}) = \bigcup_{T \in \mathscr{T}} T. \tag{1}$$

Let us consider only the mesh topologies associated with the simplex element (triangles, tetrahedra, etc.). A d-simplex is composed of $D = d + 1$ vertices. We can define ∂T the boundary of each element $T \in \mathscr{T}$ as the set of all subset of $D - 1$ nodes of T (the three edges of a triangle or the six faces of a tetrahedron). The set of faces of $\mathscr{T}$, $\mathscr{F}$, is then defined by

$$\mathscr{F}(\mathscr{T}) = \bigcup_{T \in \mathscr{T}} \partial T. \tag{2}$$

Finally, let us denote by

$$\mathscr{T}(\eta) = \{T \in \mathscr{T},\ \eta \subset T\} \tag{3}$$

the set of elements sharing a given subset of nodes η. We can introduce the following definition: $\mathscr{T}$ is a mesh topology if

$$\mathrm{card}(\mathscr{T}(F)) < 2, \quad \forall F \in \mathscr{F}(\mathscr{T}). \tag{4}$$

The boundary of $\mathscr{T}$ is

$$\partial\mathscr{T} = \{F \in \mathscr{F}(\mathscr{T}),\ \mathrm{card}(\mathscr{T}(F)) = 1\}. \tag{5}$$

2.2. Mesh topology operator

A local modification in a mesh is a cut and paste operation which is written as

$$\mathscr{T} \leftarrow \mathscr{T} - a + b, \tag{6}$$

where a is a the subset of elements in $\mathscr{T}$ to be replaced by b, another set of elements.

Let us denote by $\mathscr{E}$ the set of mesh topologies and by $\mathscr{E}(S)$ the set of mesh topologies of boundary S. In such a cut/paste operation, one has to select what piece of mesh to cut and what piece to paste. The locality of the improvement methods depends mainly on the choice of the cut operators. More precisely, in a cut/paste operation, $\mathscr{T} - a + b$, it is assumed that $a \subset \mathscr{T}$ and $b \in \mathscr{E}(\partial(a))$.

The only selected submeshes in this work are the set of common elements to a vertex or an edge: $a = \mathscr{T}(n)$ or $a = \mathscr{T}(\{n, m\})$, where n and m are nodes taken in $N(\mathscr{T})$.

Note that the edge choice includes the swapping of a diagonal in 2D but it is much more general in 3D.

In order to generate a series of mesh topologies preserving a given boundary (the necessary condition to the paste operation) a unique and simple mesh topology generator is introduced. The "staring" operator consists in connecting one node to the boundary faces which does not contain it:

$$\mathscr{T}^*(n, \partial\mathscr{T}) = \{T / T = \{\{n\} \cup F\},\ F \in \partial\mathscr{T},\ n \in \mathscr{F}\}. \tag{7}$$

The idea is to use extensively this simple generator in the selected local region. However, the cut/paste operations are restricted to a topological compatibility. Indeed it is not guaranteed that the result is still a mesh topology. In order to overcome this difficulty, we introduce $\bar{a}$, the adherence of a, defined by

$$\bar{a} = \{T \in \mathscr{T},\ T \subset \mathscr{T}(a)\}. \tag{8}$$

Finally we can define the local operator θ. Let $\eta \subset N$ and $\eta \in N$:

$$\theta^m_\eta(\mathscr{T}) = \mathscr{T} - \overline{\mathscr{T}(\eta)} + \mathscr{T}^*(n, \overline{\partial\mathscr{T}(\eta)}). \tag{9}$$

The mesh optimization algorithm consists in visiting a large number of mesh topologies determined locally by the neighbourhood of the nodes:

$$\mathscr{T}^{k+1} = \theta^{m^k}_{\{n^k\}}(\mathscr{T}^k) \tag{10}$$

or by the neighbourhood of the edges:

$$\mathscr{T}^{k+1} = \theta^{m^k}_{\{n^k_1, n^k_2\}}(\mathscr{T}^k). \tag{11}$$

The optimization process is iterated until no change is detected. In the above notation, the choice of the node (n^k, m^k), $k = 1, \ldots, \infty$, is driven first by a geometrical criterion and thereafter by an element shape factor.

2.3. Mesh generation by volume optimization

2.3.1. The minimal volume theorem

The minimal volume theorem is a very powerful tool to design a mesh generator which is based on a local optimization. Let us associate coordinates via a mapping from the set of nodes to $\mathbb{R}^d$:

$$X : N \to \mathbb{R}^d \quad (d = 2, 3). \tag{12}$$

Let us denote by $X(T)$, the set of D vertices associated with T and by Ω_T the d-simplex, the convex hull of these D points. These simplex generate the domain $\Omega(\mathscr{T}, X)$ since the boundary faces generate the surface $\Gamma(\partial\mathscr{T}, X)$:

$$\Omega(\mathscr{T}, X) = \bigcup_{T \in \mathscr{T}} \Omega_T, \tag{13}$$

$$\Gamma(\partial\mathscr{T}, X) = \bigcup_{F \in \partial\mathscr{T}} \Gamma_T. \tag{14}$$

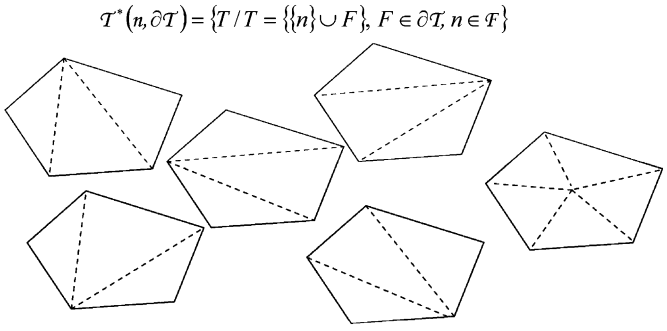

Fig. 1. Different candidate mesh topologies provided by the staring operator (which tries to connect a node to boundary faces).

The general case makes that $\Gamma(\partial\mathscr{T},X)$ differs from $\partial\Omega(\mathscr{T},X)$ but the following result shows when these two objects are the same. Let us consider a domain Ω which boundary is defined by conformal triangulation. We assume that $\Gamma(\partial\mathscr{T},X)=\partial\Omega$ and that $\mathscr{T}$ is oriented.

Let $(\mathscr{T},X)$ be as above, $\mathscr{T}$ being oriented. We assume that $(\mathscr{T},X)$ provides a conformal triangulation of the domain Ω (i.e. $\Gamma(\partial\mathscr{T},X)=\partial\Omega$). Then:

(a) $\sum_{T\in\mathscr{T}}|\Omega_T|\geqslant|\Omega|$.
(b) $(\mathscr{T},X)$ is a mesh of Ω if and only if: $\sum_{T\in\mathscr{T}}|\Omega_T|=|\Omega|$ and $|\Omega_T|>0,\ \forall T\in\mathscr{T}$.

The proof is given in [15].

2.3.2. Selection based on minimal volume

If we consider a subpart of the mesh (S,X), and the nodes reached by it, $N=N(S)$, we are looking first for the candidate mesh topologies of minimal volume. Indeed, by defining:

$$\text{Volume}(a)=\sum_{T\in a}|\Omega_T| \tag{15}$$

and by introducing:

$$N^*(a)=\left\{n\in N(a),\ \text{Volume}(T^*(n,\partial a))=\min_{i\in N(a)}\ \text{Volume}(T^*(i,\partial a))\right\}, \tag{16}$$

we precisely select the candidates of minimal volume and consequently those which are susceptible to provide a conformal mesh (or at least which tend to a conformal). Among these possible candidates, it remains to choose the best one in terms of a quality objective.

2.3.3. The best selection

The shape factor of a simplex can be defined by the following function:

$$c(X,T)=\frac{|\Omega_T|}{h(T)^d}, \tag{17}$$

where h measures the edge length:

$$h(X,T)=\sum_{i,j\in T}||X(i)-X(j)||. \tag{18}$$

The shape factor enables to sort the elements from the worse to the best within a submesh by

$$T=a_i\in a,\quad i=1,\ldots,|a|,\ c(a_i)\leqslant c(a_{i+1}) \tag{19}$$

and two subset of elements a and b can be compared by means of their worse elements:

$$a<b\iff\exists e,\ \forall i<e,\ a_i=b_i,\quad\text{and}\quad a_e<b_e. \tag{20}$$

The procedure described defines the exact mechanism of selection at each step of improvement.

2.4. Node generation, node deletion and mesh size map enforcement

The node generation is simply done by adding a new node candidate in the list of submesh topology built with the help of the staring operator (Fig. 1). This new node is associated with the coordinate of the barycentre of the current visited subdomain. A refinement (or coarsening) process is accounted for enforcing a mesh size map. In fact the mesh size is taken into account by two possible ways. The first one is to transform the local space in such a way that the element size must be equal to unity, see [16]. The second almost equivalent solution is to modify the shape factor (Figs. 2 and 3).

Let H be a mesh size mapping function and $\mathscr{M}=(\mathscr{T},X)$ a mesh of Ω. The mesh size map is naturally defined at the element level. We choose to interpolate continuously the mesh size in order to have nodal values. Then the required mesh size on a given element is just the average value obtained from the nodal values.

$$H_T=\sum_{i\in T}H_h(X(i))/D. \tag{21}$$

The adaptive process consists in improving the mesh until the interpolated mesh size map and the current element size correspond. For that purpose we change the shape factor by

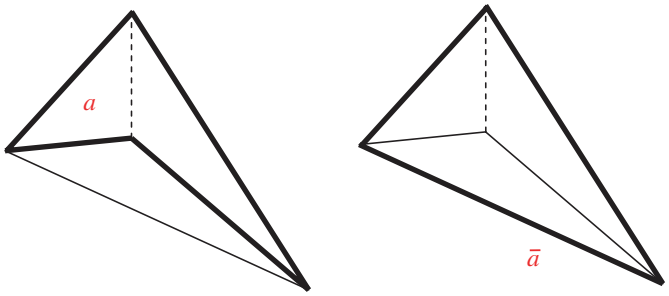

Fig. 2. Swapping the diagonal (dot line) is not allowed because the resulting edge already exists in the mesh. Working with $\bar{a}$ avoids to have to detect such a situation.

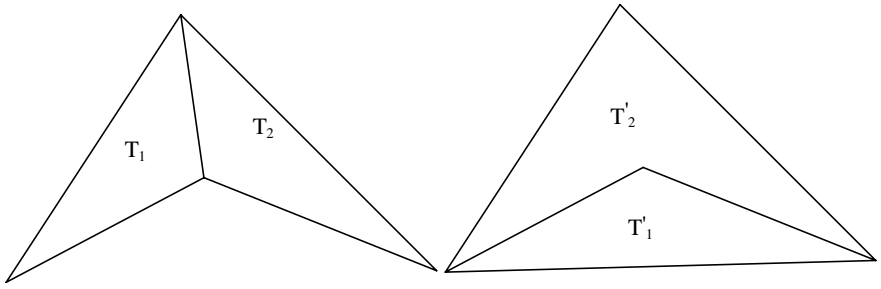

Fig. 3. Two valid mesh topologies, but the only valid mesh configuration is determined by a minimal volume criterion: volume(T'_1) + volume$(T'_2 >$ volume(T_1) + volume(T_2)).

$$C(X,T,H_T) = \frac{\min(|\Omega_T|, |\omega(H_T)|)}{\max(|\Omega_T|, |\omega(H_T)|)} c(X,T), \tag{22}$$

where $|\omega(H_T)|$ is the volume of the equilateral simplex of size H_T.

The advantage of continuous interpolation of the mesh size map is mainly due to the fact that it is defined by its nodal value. The mesh topology changes do not affect the nodal value of the mesh size map. When a node is created it is associated with a local average value of the require mesh size.

Remark. The surface mesh and the volume mesh are strongly coupled by inserting a layer of virtual elements (or boundary elements). This virtual layer is a trick to close the mesh topology in such a way that there are no more boundaries. A new constraint is added in the process of optimization: the volume of these virtual boundary elements is forced to remain null. The virtual layer is simply performed by connecting every boundary node to a unique virtual node (a particular number). The geometry is preserved by controlling the thickness of the virtual boundary elements. These elements are those containing the virtual node. This enables to modify the actual boundary mesh while preserving the geometry integrity.

3. A posteriori error estimation

For a flow formulation, the error due to the finite element approximation can be expressed in any suitable norm as the difference between the exact velocity solution field v and the finite element one v_h:

$$\|e_h\| = \|v - v_h\|. \tag{23}$$

The energy norm is generally preferred for engineering applications. For incompressible materials, the error related to the spherical part of the stress tensor, the pressure p, is neglected [12,17], so the selected norm is written as

$$\|e_h\|_E = \|s - s_h\|_E = \left(\int_\Omega (s - s_h) : (\dot{\varepsilon} - \dot{\varepsilon}_h) \, \mathrm{d}\omega \right)^{1/2} = \left(\int_\Omega \varsigma(s)^{-1} (s - s_h) : (s - s_h) \, \mathrm{d}\omega \right)^{1/2}, \tag{24}$$

where $(s, \dot{\varepsilon})$ are the exact deviatoric stress and strain rate tensors, $(s_h, \dot{\varepsilon}_h)$ are the corresponding discretized ones, and $\varsigma(s)$ is the material viscosity $(s = \varsigma(\dot{\varepsilon})\dot{\varepsilon})$. To evaluate the error it is more convenient to use a relative value:

$$\eta_h = \frac{\|e_h\|_E}{\left(\int_\Omega s : \dot{\varepsilon}\, \mathrm{d}\omega\right)^{1/2}}. \tag{25}$$

In the SPR Zienkiewicz–Zhu (Z^2) [8] approach, the exact error is estimated by approximating the exact solution s by a recovered superconvergent solution $\tilde{s}_h$ that is computed from the finite element one s_h. The estimation is then written:

$$\theta^{Z^2} = \|\tilde{e}_h\|_E = \left(\int_\Omega \varsigma(s_h)^{-1}(\tilde{s}_h - s_h) : (\tilde{s}_h - s_h)\, \mathrm{d}\omega\right)^{1/2}. \tag{26}$$

The reliability of the estimation is evaluated by its efficiency index ξ:

$$\xi = \frac{\|\tilde{e}_h\|_E}{\|e_h\|_E}. \tag{27}$$

The error estimator is asymptotically exact if ξ converges to unity as the mesh is refined, i.e. if the exact error tends to zero. For the Z^2 error estimator it is easily shown that [18]

$$1 - \frac{\|\tilde{e}_h\|_E}{\|e_h\|_E} \leqslant \xi \leqslant 1 + \frac{\|\tilde{e}_h\|_E}{\|e_h\|_E}. \tag{28}$$

If the convergence rate of the recovered solution $\tilde{s}_h$ is higher than the finite element one s_h, $\|\tilde{e}_h\|_E$ tends to zero faster than the finite element one $\|e_h\|_E$, and the Z^2 error estimator is asymptotically exact.

3.1. Size maps for adaptive remeshing strategies

The optimality condition of the new mesh requires that the error is uniformly distributed among the new elements. The standard adaptive remeshing strategy, AST1, determines an optimized mesh T^{opt} that should satisfy a prescribed global accuracy θ^{imp}:

Let θ_e be the contribution of the element e to the global estimated error θ satisfying:

$$\theta = \left(\sum_e^{\mathrm{Nbelt}} \theta_e^2\right)^{1/2}, \tag{29}$$

where Nbelt is the total number of elements of the mesh. If the convergence rate of the finite element method is supposed to be uniform and equal to p on the whole domain, the optimal size h_e^{opt} of the element e is computed by

$$\frac{\theta_e^{\mathrm{opt}}}{\theta_e} = \left(\frac{h_e^{\mathrm{opt}}}{h_e}\right)^p, \tag{30}$$

$$\theta^{\mathrm{imp}} = \left(\sum_e^{\mathrm{Nbelt}} (\theta_e^{\mathrm{opt}})^2\right)^{1/2}, \tag{31}$$

where θ_e^{opt} is the contribution of the element e of the optimal mesh to the global estimated error and h_e is the size of the element e. For a linear interpolation and a linear constitutive model the theoretical value of p is 1. For non-linear constitutive models, it is supposed to remain close to 1. In 3D, the number of elements of the optimal mesh is given by

$$\mathrm{Nbelt}^{\mathrm{opt}} = \sum_e^{\mathrm{Nbelt}} \left(\frac{h_e^{\mathrm{opt}}}{h_e}\right)^{-3}. \tag{32}$$

The optimality condition for the new mesh, that is to say the minimisation of the number of elements (32), requires that the error is uniformly distributed on each new element. The value of the uniformly distributed error θ^{uni} is given by

$$\theta^{\mathrm{uni}} = (\theta^{\mathrm{imp}})^{\frac{2p+3}{2p}} \left(\sum_e^{\mathrm{Nbelt}} (\theta_e)^{\frac{6}{2p+3}}\right)^{-\frac{2p+3}{4p}}, \tag{33}$$

which leads to the determination of the optimal size of the element:

$$h_e^{\mathrm{opt}} = \left(\frac{\theta^{\mathrm{uni}}}{\theta_e}\right)^{\frac{2}{2p+3}} h_e. \tag{34}$$

For practical applications and especially for forging problems, the material flow becomes more and more complex along the process. So, maintaining a prescribed accuracy results into rapidly increasing the number of elements in the optimized mesh T^{opt}. The computational cost becomes higher and higher and there is a risk to exceed computer and mesh generator capabilities. The idea is then to take into account the limitations of computer resources. This second approach, AST2, consists in the determination of an optimized mesh T^{opt} for a prescribed number of elements $\text{Nbelt}^{\text{imp}}$ and the best accuracy. The new optimal element size is still given by (34) but with the value of the global accuracy θ^{imp} as follows:

$$\theta^{\text{imp}} = (\text{Nbelt}^{\text{imp}})^{-\frac{p}{3}} \left(\sum_{e}^{\text{Nbelt}} (\theta_e)^{\frac{6}{2p+3}} \right)^{\frac{2p+3}{6}}. \tag{35}$$

Coorevits et al. [19] propose a similar approach with the definition of the computation constrains: *a prescribed memory size* of the computer or *a prescribed CPU time* with a maximum of accuracy, which provides an indirect way to define $\text{Nbelt}^{\text{imp}}$.

In practice, these two strategies are combined (see the algorithm in the following paragraph). The size map is defined on the elements, so if the mesh is too coarse then the map is not quite accurate and the refinement rate of some elements, h_e^{opt}/h_e, can be very small (or very large). It can result into strong gradients of the mesh size, suggesting connecting elements of very different sizes which is not feasible. It means that the refinement is too strong and that an intermediate mesh must be created to better evaluate the mesh size map. This limitation is taken into account by introducing an additional condition to limit the refinement rate at each remeshing step (Fig. 4):

$$\alpha \leqslant \frac{h_e^{\text{opt}}}{h_e} \leqslant \beta \quad \text{with } \alpha < 1 < \beta, \tag{36}$$

where α and β are numerically determined to satisfy the mesh generator capabilities. In practice we use $\alpha = 0.25$ and $\beta = 2$.

The following algorithm is used for the determination of the optimal mesh T^{opt}:

(i) Compute the error estimation and its element contributions.
(ii) Compute h_e^{opt} for any element of the mesh with the AST1 strategy and satisfying (36).
(iii) Compute the new number of elements $\text{Nbelt}^{\text{opt}}$ with (32):
- If $\text{Nbelt}^{\text{opt}} \leqslant \text{Nbelt}^{\text{imp}}$ then the new mesh is accepted.
- Else:
  - Use a dichotomy algorithm to compute θ^{imp} ensuring that $\text{Nbelt}^{\text{opt}} \approx \text{Nbelt}^{\text{imp}}$, taking into account the condition (36).
  - Compute a new mesh size map with the AST2 strategy.

4. Error estimation

4.1. Superconvergent patch recovery (SPR)

The SPR method is based on a continuous polynomial expansion of the stress tensor on a finite element patch (see Fig. 5). This expansion is obtained by a local least square fit of the stresses at supposingly superconvergent Gauss points of the patch. For some problem, it has been shown [20,21] that the convergence rate of the derivatives is higher than the global finite element rate at some points. However, for triangles and tetrahedra, the location of superconvergent points is not fully explored mathematically. Zienkiewicz and Zhu [8] propose to use the "optimal points" which are located at the centre of linear elements. This choice is also justified and recommended by Babuška et al. [22] by exhaustive numerical investigations. So, in the present study, integration Gauss points that are located at the centre of the linear tetrahedra are used.

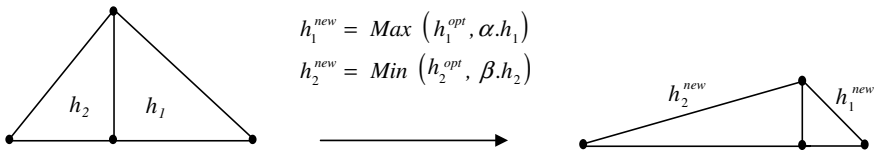

Fig. 4. Size modification limits.

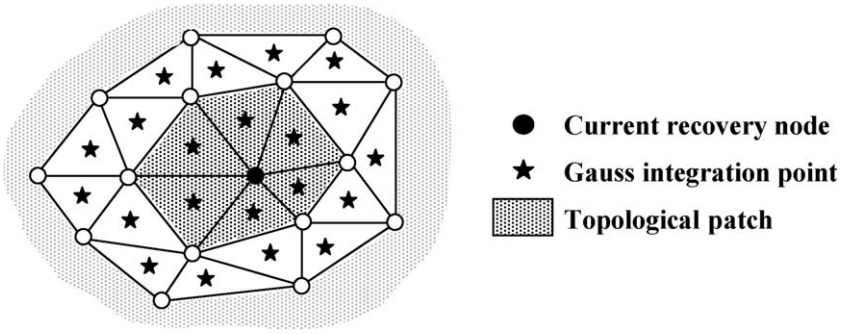

Fig. 5. Superconvergent patches for linear elements and 2D problem.

The deviatoric part of the recovered stress tensor is continuously interpolated over the domain using the same interpolation functions N^k as the primal (velocity and pressure) variables [23]:

$$\tilde{s}_h = \sum_k \tilde{s}^k N^k, \tag{37}$$

where $\tilde{s}^k$ is the recovered solution at node k computed by considering a polynomial expansion of the stress field $\tilde{s}_h^k$ in the FE patch (or topological patch) centred on k:

$$\tilde{s}_h^k = P \cdot a^k, \tag{38}$$

where P contains the polynomial terms of expansion and a^k is the vector of unknown parameters. For a 3D problem and for a linear interpolation we write:

$$P = [1, x, y, z] \quad \text{and} \quad a^k = \left[a_1^k, a_2^k, a_3^k, a_4^k\right]^t. \tag{39}$$

The unknown coefficients a_i^k are determined by the minimization of a least square functional as follows:

$$\Pi = \sum_i^n (s_h(x_i, y_i, z_i) - \tilde{s}_h(x_i, y_i, z_i))^2, \tag{40}$$

where n is the number of sampling points (integrations points at the centre of the elements) inside the patch (see Fig. 5), (x_i, y_i, z_i) their coordinates. and $s_h(x_i, y_i, z_i)$ is the value of the finite element field at these points.

The solution of this problem is given by a linear system:

$$A \cdot x = b, \tag{41}$$

where:

$$A = \sum_i^n \begin{pmatrix} 1 & x_i & y_i & z_i \\ x_i & (x_i)^2 & x_i y_i & x_i z_i \\ y_i & y_i x_i & (y_i)^2 & y_i z_i \\ z_i & z_i x_i & z_i y_i & (z_i)^2 \end{pmatrix} \quad \text{and} \quad x = \begin{pmatrix} a_1^k \\ a_2^k \\ a_3^k \\ a_4^k \end{pmatrix} \quad \text{and} \quad b = \sum_i^n s_h(x_i, y_i, z_i) \begin{pmatrix} 1 \\ x_i \\ y_i \\ z_i \end{pmatrix}, \tag{42}$$

$\tilde{s}^k$ is then computed by the value of $\tilde{s}_h^k$ at the centre of the patch.

For interior nodes the number of equations of the minimization problem is higher than the number of unknowns a_i^k and the matrix A is positive definite. However, for boundary nodes, the number of sampling points may not be enough to solve the minimization problem, as $\tilde{s}^k$ cannot be determined by using the patch centred on k. So another interior patch centred on the nearest internal node l is used. Finally $\tilde{s}^k$ is the value of $\tilde{s}_h^l$ at node k [18].

4.2. Mechanical formulation of the forging problem

The presented mesh adaptive procedure is applied to non-steady metal forming problems, whose basic equations are presented here.

In forging problems elasticity effects can be neglected and an incompressible rigid viscoplastic model is often considered, like the isotropic Norton–Hoff constitutive equation:

$$s = 2K(\sqrt{3}\dot{\bar{\varepsilon}})^{m-1}\dot{\varepsilon} \quad \text{and} \quad \operatorname{div} v = \operatorname{tr}\dot{\varepsilon} = 0, \tag{43}$$

where $\dot{\varepsilon}$ is the strain rate tensor, K is the material consistency, which may be a function of strain hardening and temperature, and m is the strain rate sensitivity coefficient and $\dot{\bar{\varepsilon}}$ is the equivalent strain rate:

$$\dot{\bar{\varepsilon}} = \left(\frac{2}{3}\sum_{i,j}\dot{\varepsilon}_{ij}^2\right)^{1/2}. \tag{44}$$

A Coulomb friction law is considered at the interface $\partial_c\Omega$ between the dies and the workpiece Ω (Fig. 6):

$$\tau = -\mu\sigma_n\frac{\Delta v_t}{\|\Delta v_t\|} \text{ if } |\mu\sigma_n| \leqslant \bar{m}\frac{\sigma_0}{\sqrt{3}} \quad \text{and} \quad \tau = \bar{m}\frac{\sigma_0}{\sqrt{3}}\frac{\Delta v_t}{\|\Delta v_t\|} \text{ if } |\mu\sigma_n| > \bar{m}\frac{\sigma_0}{\sqrt{3}}, \tag{45}$$

where n is the normal to the die, σ_0 is the material yield stress, $\bar{m}$ is the Tresca coefficient and Δv_t is the relative tangential velocity defined as

$$\Delta v_t = v - v_d - [(v - v_d)\cdot n]\cdot n, \tag{46}$$

where v_d is the imposed die velocity.

A Norton viscoplastic friction law is also frequently used:

$$\tau = -\alpha K|\Delta v_t|^{q-1}\Delta v_t \quad \text{on } \partial_c\Omega, \tag{47}$$

where α and q are friction coefficients.

The non-penetrability condition between dies and workpiece is written on the contact boundary $\partial_c\Omega$ of Ω as follows:

$$(u - u_d)\cdot n \leqslant \delta \quad \text{on } \partial_c\Omega, \tag{48}$$

where u and u_d are respectively the displacement field and the die displacement. δ is a signed distance to the surface.

The balance equation when inertia and body forces are neglected is

$$\operatorname{div}(\sigma) = 0. \tag{49}$$

The virtual work principle is written in a mixed form. It provides the integral form, which holds for any virtual cinematically admissible velocity field v^* (which verifies $v^*\cdot n = 0$ on $\partial_c\Omega$) and any virtual pressure field p^*:

$$\int_\Omega s : \dot{\varepsilon}^*\,\mathrm{d}\omega - \int_\Omega p\cdot\operatorname{div}(v^*)\,\mathrm{d}\omega - \int_{\partial_c\Omega}\tau\cdot v^*\,\mathrm{d}s = 0, \tag{50}$$

$$-\int_\Omega p^*\cdot\operatorname{div}(v)\,\mathrm{d}\omega = 0, \tag{51}$$

where v is a cinematically admissible field which satisfies (48).

The problem is discretized by the finite element method, using P1+/P1 interpolation for the velocity and pressure fields:

$$\begin{aligned} v_h &= \sum_k^{\text{Nbnoe}} v_k N^k + \sum_e^{\text{Nbelt}} \bar{v}_e b^e, \\ p_h &= \sum_k^{\text{Nbnoe}} p_k N^k, \end{aligned} \tag{52}$$

where v_k and p_k are the nodal velocity and pressure values. Nbnoe and Nbelt are respectively the number of nodes and elements. N^k is the interpolation functions and $\bar{v}_e$ are the degrees of freedom associated with the bubble functions b^e.

The contact conditions for any node of $\partial_c\Omega$ are handled by a penalty formulation.

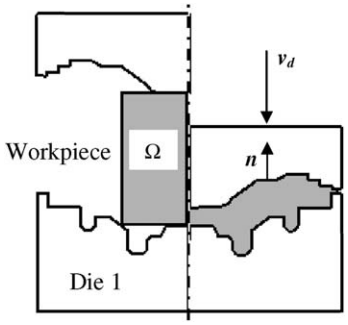

Fig. 6. Domain Ω and dies.

An updated Lagrangian formulation is used for non-steady process and an implicit Euler Scheme for time integration is adopted:

$$x_h^{t+\Delta t} = x_h^t + v_h^{t+\Delta t}\Delta t, \tag{53}$$

where Δt is the time step.

4.3. Estimator efficiency for benchmark extrusion problem

A numerical study on the efficiency of the recovery procedure is carried out to evaluate the Z^2 error estimator for a mixed formulation, non-linear constitutive equations and a 3D frame. The present study does not intend to be sufficient to accurately evaluate the Z^2 efficiency in viscoplasticity. Other numerical investigations have been carried out for different non-linear problems bringing to the same conclusions. Both the efficiency of the recovery procedure and the error estimator are evaluated. The recovery effectivity index is defined as follows:

$$\beta = \frac{\|s - s_h\|_E}{\|s - \tilde{s}_h\|_E}, \tag{54}$$

where $\|s - s_h\|_E$ is the exact finite element error and $\|s - \tilde{s}_h\|_E$ is the recovered error. The recovery procedure is said to be effective if $\beta > 1$.

The studied problem regards a metal extrusion process (Fig. 7). The billet undergoes a 60–20 mm reduction of section. The extrusion speed is $v_d = 15$ mm/s.

For symmetry reasons, only the half of the workpiece is considered. The contact between dies and workpiece is perfectly sticking. The material behaviour is viscoplastic according to Eq. (43) where $m = 0.14$ and the material consistency K depends on the temperature and the total deformation as follows:

$$K(T, \bar{\varepsilon}) = K_0(\bar{\varepsilon} + \varepsilon_0)^n \exp\left(\frac{\beta}{T}\right), \tag{55}$$

where $\bar{\varepsilon}$ is the total equivalent strain, ε_0 is a numerical coefficient, T is the temperature, n is the coefficient of the sensitivity to the strain-hardening and β is the temperature softening coefficient. For the numerical application the following values are adopted: $K_0 = 1.625 \times 10^3$ MPa, $\beta = 2.5 \times 10^3$, $n = 0.174$, $\varepsilon_0 = 10^{-4}$.

The initial workpiece and dies temperatures are respectively 750 °C and 50 °C.

Four structured embedded meshes, with uniform refinement and increasing number of nodes (Fig. 8), are used for the FE calculations. Since the exact solution of the problem is unknown, the solution of the finest mesh (reference mesh) is regarded as the exact one. Numerical results are summarized in Table 1 and Fig. 9.

It is noticed that the Z^2 effectivity index converges asymptotically to 0.8, which indicates that the estimator underestimates the error by 20%. In the adaptive procedure, a correcting factor is then required. In this case the estimated error is multiplied by a factor of 1.25. On the other hand, Table 1 shows that the recovery effectivity index is always higher than 1, and that the recovery process is more efficient when the mesh size increases, that is to say, when the quality of the finite element solution decreases. In practice, it is an important property, as Zienkiewicz and Zhu [10] have shown, that even if the superconvergence does not occur, a good estimator is obtained when the recovery process gives a more accurate

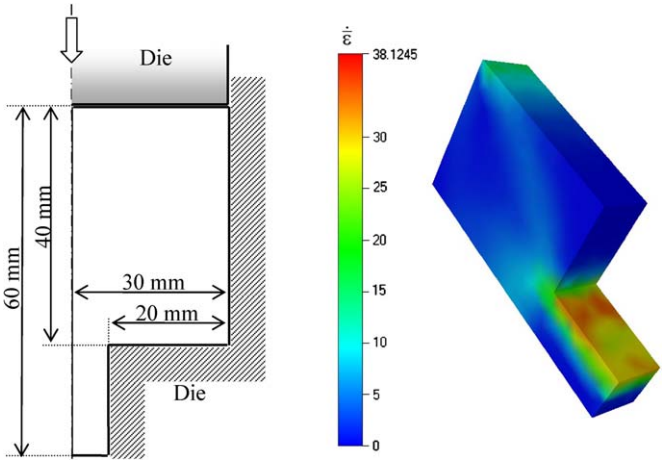

Fig. 7. Extrusion problem and 3D mesh.

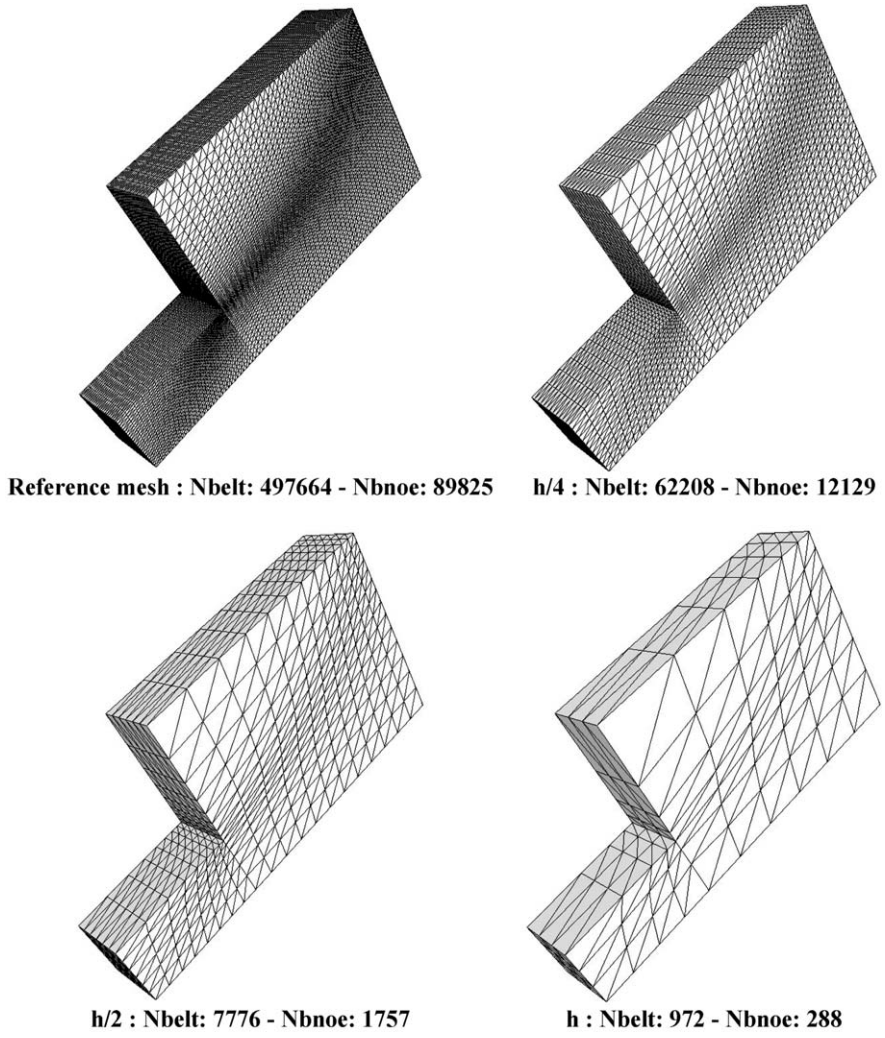

Fig. 8. Finite element meshes for the validation problem.

Table 1
Errors and global effectivity indexes

Mesh	$\|s - s_h\|_E$ (%)	$\|s - \tilde{s}_h\|_E$ (%)	$\|\tilde{s}_h - s_h\|_E$ (%)	ξ	β
$h/4$	18.35	13.63	15.40	0.84	1.35
$h/2$	28.38	20.50	25.00	0.88	1.38
h	46.95	30.35	47.52	1.01	1.55

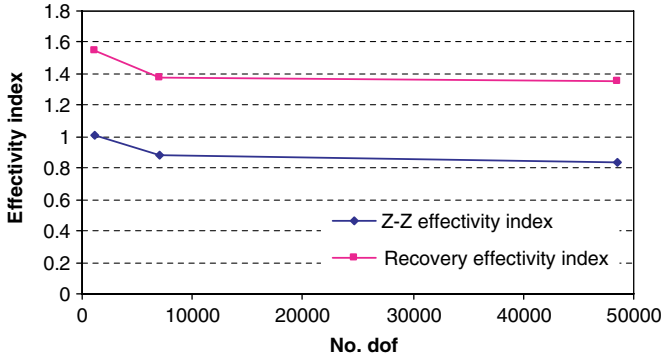

Fig. 9. Global effectivity indexes.

answer than the FE approximation. Therefore, this benchmark test shows that the SPR estimator is efficient for mixed velocity/pressure formulations with non-linear viscoplastic law and in a 3D frame, although the extrusion problem provides a complex flow, with singularity in the angle, which explains that the convergence rate of the finite element method is less than 1 in the energy norm.

5. Application to 3D forging

In this section error estimation and determination of optimized meshes are carried out. The size map for the mesh generator is constructed by nodal averaging of the element sizes computed from (34). The remeshing procedure is activated by different remeshing criteria:

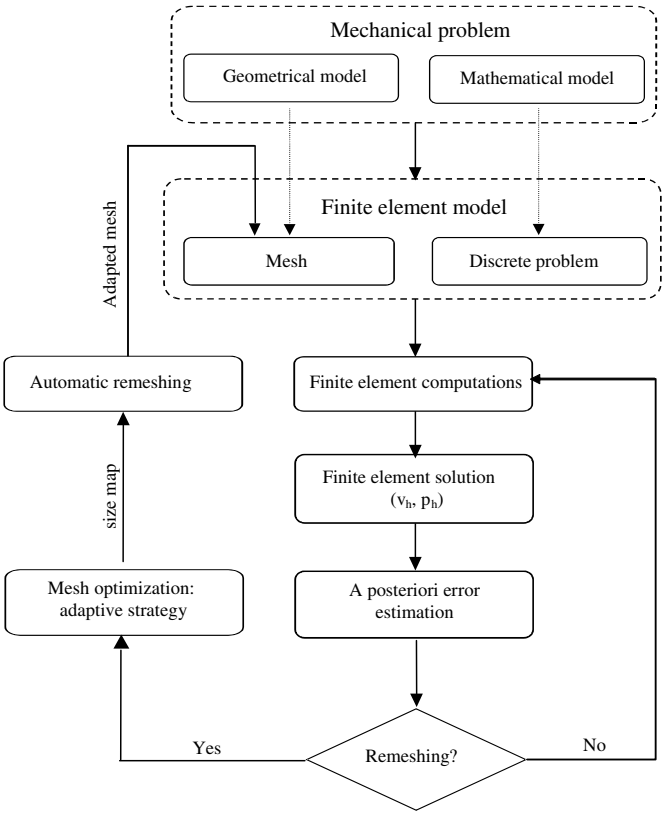

Fig. 10. Simulation algorithm diagram.

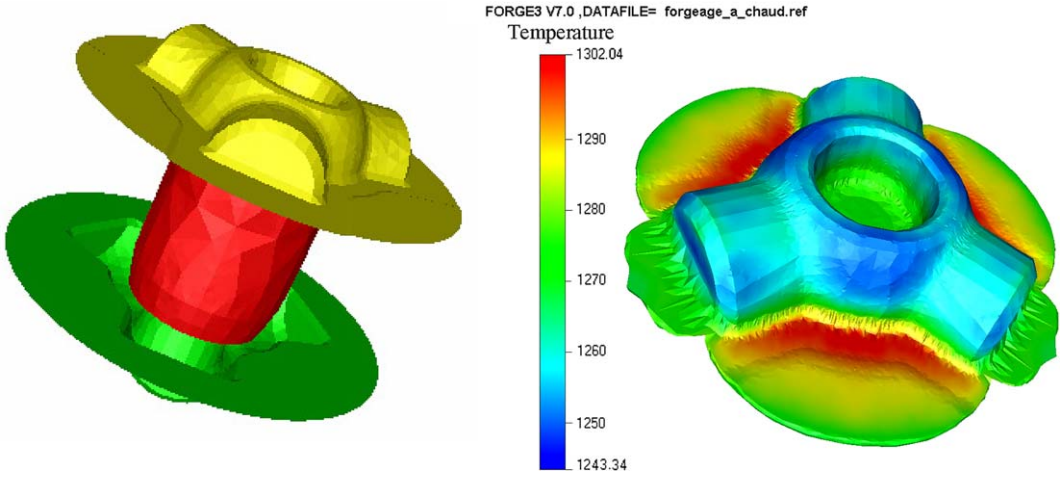

Fig. 11. Forging simulation of a spindle: initial perform and final part.

- Remeshing due to an increase of the total strain since last remeshing, which allows adapting the mesh when important deformation occurs.
- Remeshing due to volume element quality when an element of the mesh is distorted.
- Periodic remeshing after a prescribed number of increments.
- Remeshing due to penetration between dies and the segments of the mesh.

At every time step, the error is estimated and the optimized map size is determined in order to be available when a remeshing criterion is satisfied (Fig. 10).

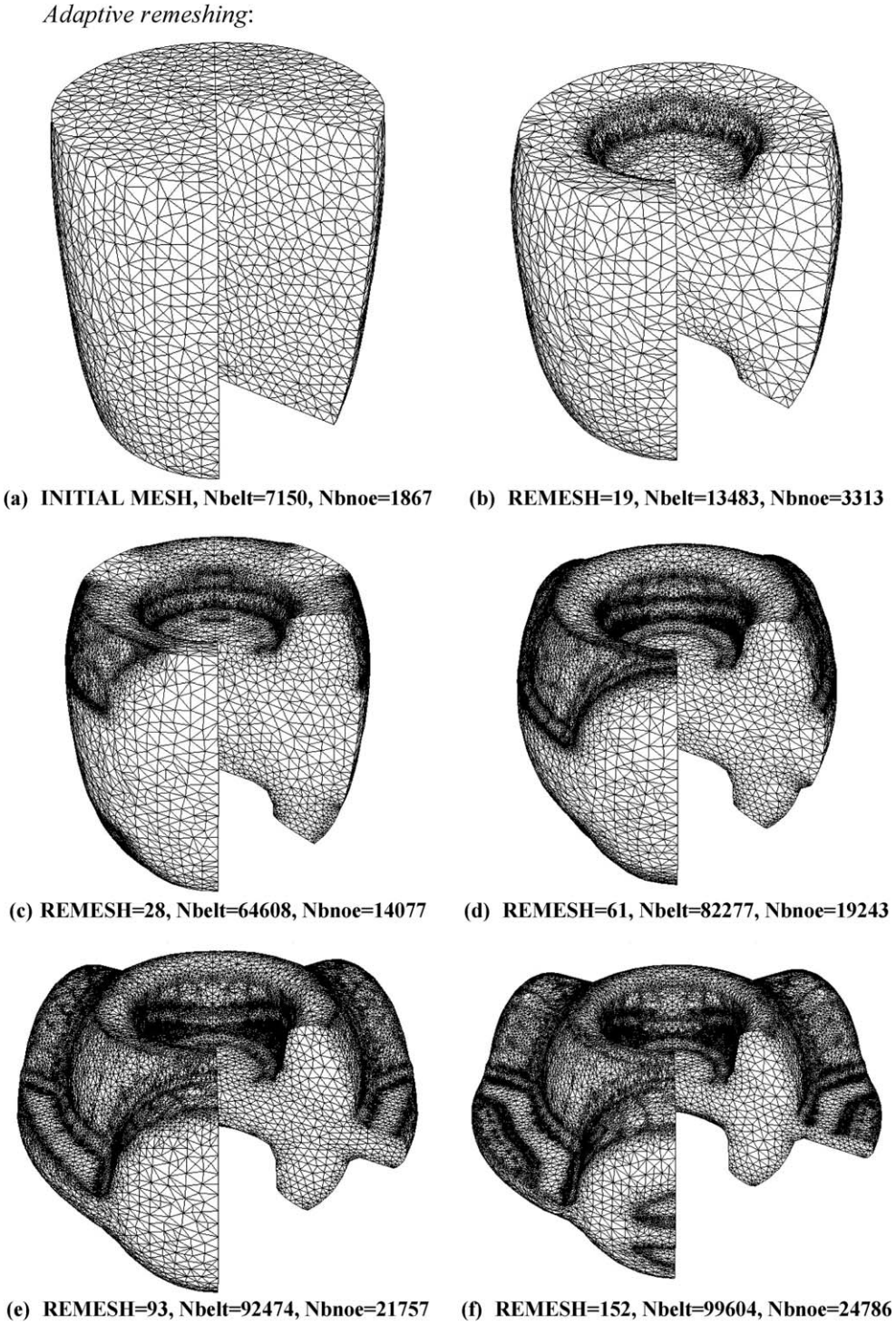

Fig. 12. Adaptive remeshing for the spindle forging simulation.

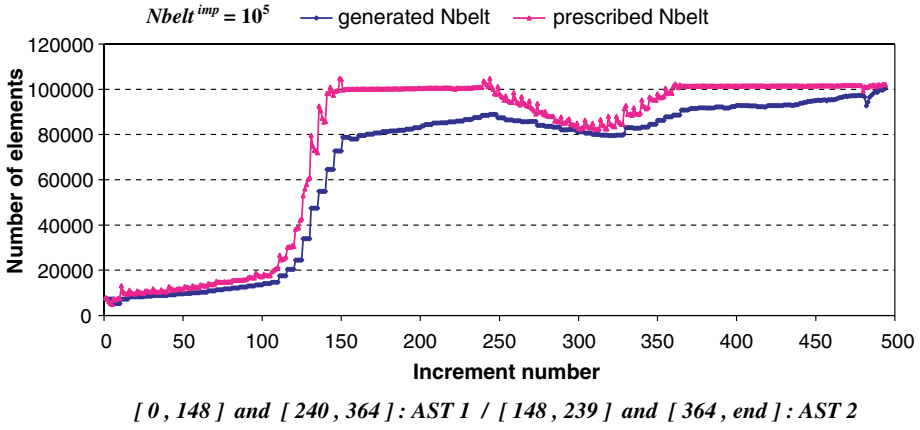

Fig. 13. Evolution of the number of element spindle forging simulation.

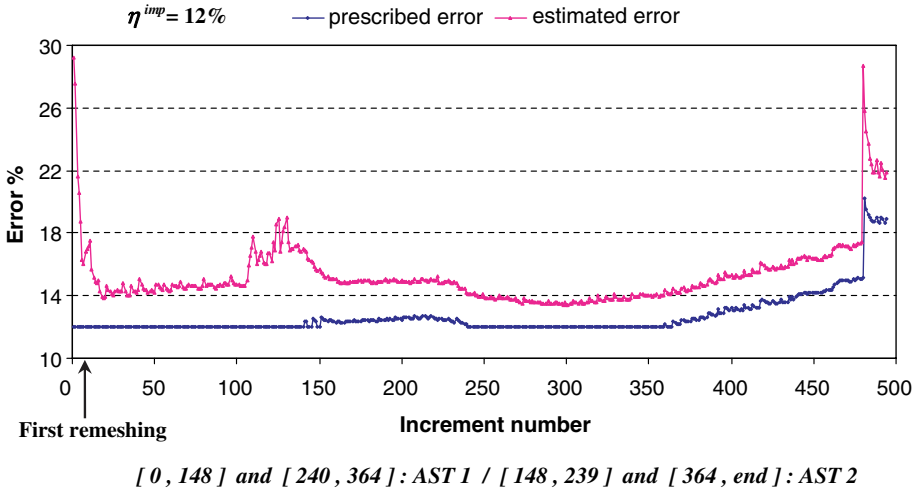

Fig. 14. Evolution of the estimated error during forging simulation of spindle.

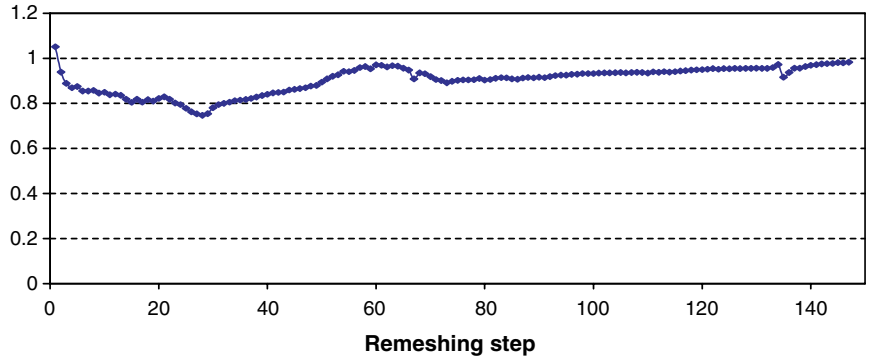

Fig. 15. Ratio between the obtained and the prescribed number of elements during forging simulation of a spindle.

5.1. Forging of spindle

5.1.1. Adaptive remeshing in workpiece

The Hot forging of a "spindle" is simulated (see Fig. 11), with the FORGE3® software. The material is supposed to obey the Norton–Hoff constitutive equation (43) with $m = 0.139$ K defined by (55) with: $K_0 = 1.49 \times 10^3$ MPa,

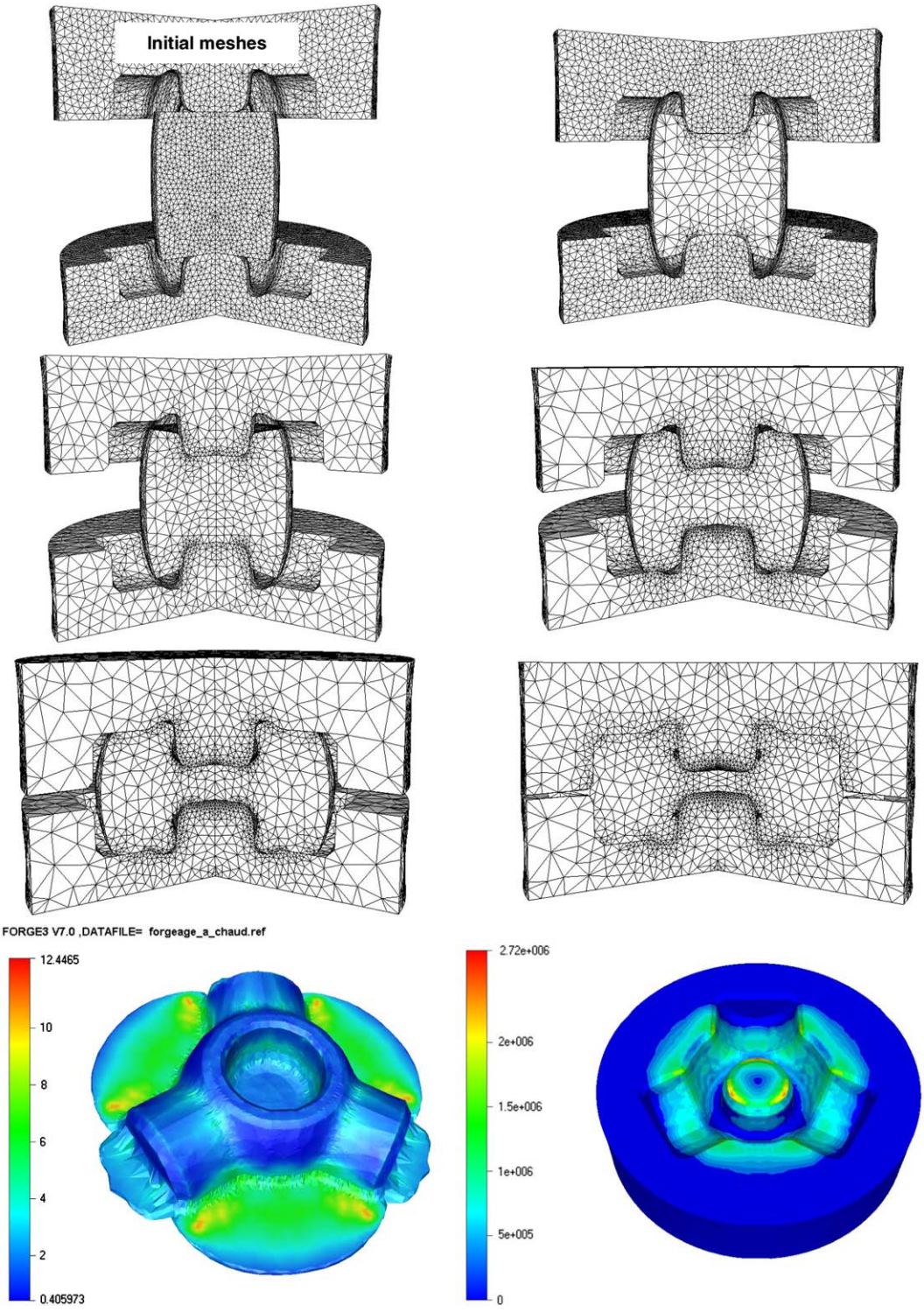

Fig. 16. Adaptive remeshing in dies and workpiece and isovalues of the equivalent deformation in the workpiece and damage in the lower die.

$\beta = 2.9 \times 10^{-3}$, $n = 0.1123$, $\varepsilon_0 = 10^{-4}$. The initial part and dies temperatures are respectively 1250 °C and 250 °C. A Coulomb friction law (45), with the adopted parameters: $\bar{m} = 0.3$ and $\mu = 0.15$. For mesh adaptivity, the imposed relative error is $\eta^{\text{imp}} = 12\%$ and the imposed maximum number of elements in the mesh is $\text{Nbelt}^{\text{imp}} = 100{,}000$. Remeshing is activated every 10 increments or when another remeshing criterion is satisfied.

The numerical results presented in Figs. 12–14 show the efficiency of the adaptive remeshing strategy. From the beginning of the simulation to increment 148 the AST1 strategy is activated with $\eta^{\text{imp}} = 12\%$. Fig. 13 shows a large increase of the number of elements which reaches the imposed maximum value 100,000 at the increment 149. Then the AST2 strategy

is used up to increment 239. During this step, the imposed error is allowed to be higher than 12% in order to maintain the number of elements less than $Nbelt^{imp}$. This alternation between the two strategies provides a robust way to produce the best possible mesh for a given computational cost. Fig. 14 shows a good correlation between the imposed and actually estimated errors, and how it is therefore possible to control the error. Fig. 13 shows the good prediction of the number of elements (32) and the capability of the mesh generator to follow this criterion, so making it possible to control the problem size.

Fig. 15 shows the evolution of the ratio between the number of elements in the adapted meshes (generated Nbelt) and the prescribed one (prescribed Nbelt). This ratio is globally close to 0.9, which indicates the robustness of the mesh generator. The ratio is always less or equal than 1 and therefore the obtained number of elements does not exceed the prescribed value.

5.1.2. Adaptive remeshing in dies and workpiece

Forge3® makes it possible to carry out computations in the forging tools which are assumed to have an elastic behaviour. This may be very useful to study tool damage for instance. Adaptive remeshing in the tools is carried out in the same way as in the workpiece. For elasticity problem the Z^2 error estimator is written as

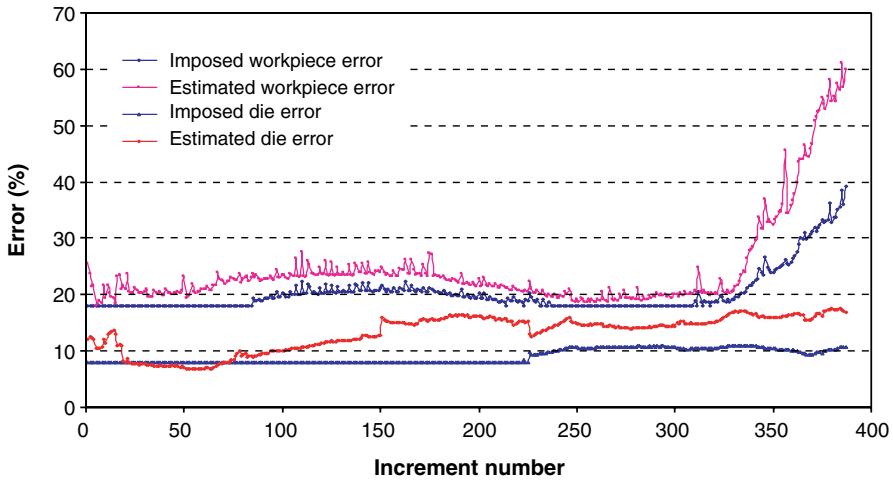

Fig. 17. Evolution of the estimated error in the workpiece and lower die during the forging simulation of a spindle.

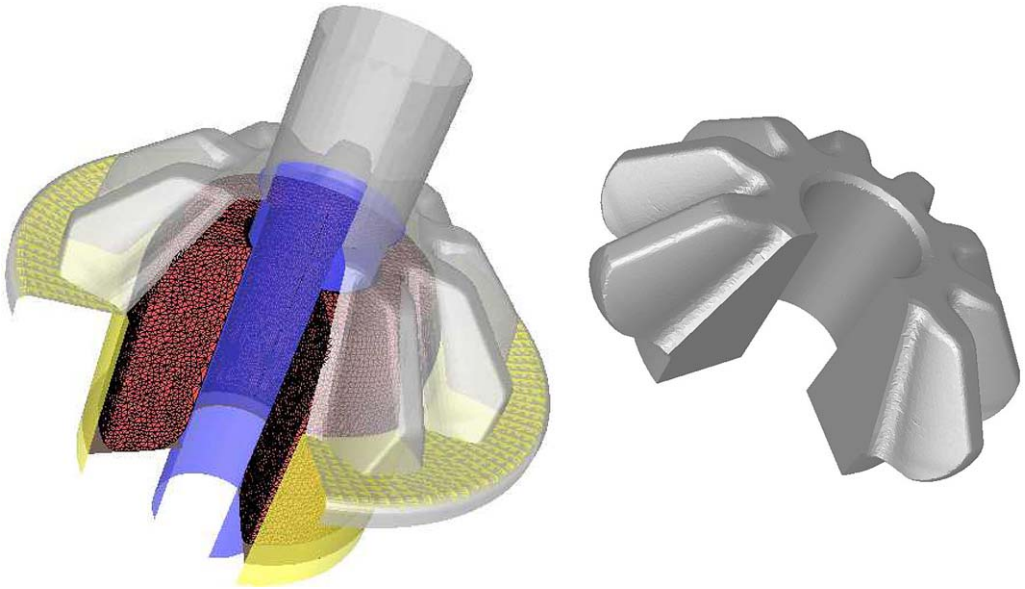

Fig. 18. Forging simulation of a gear: initial preform and final part.

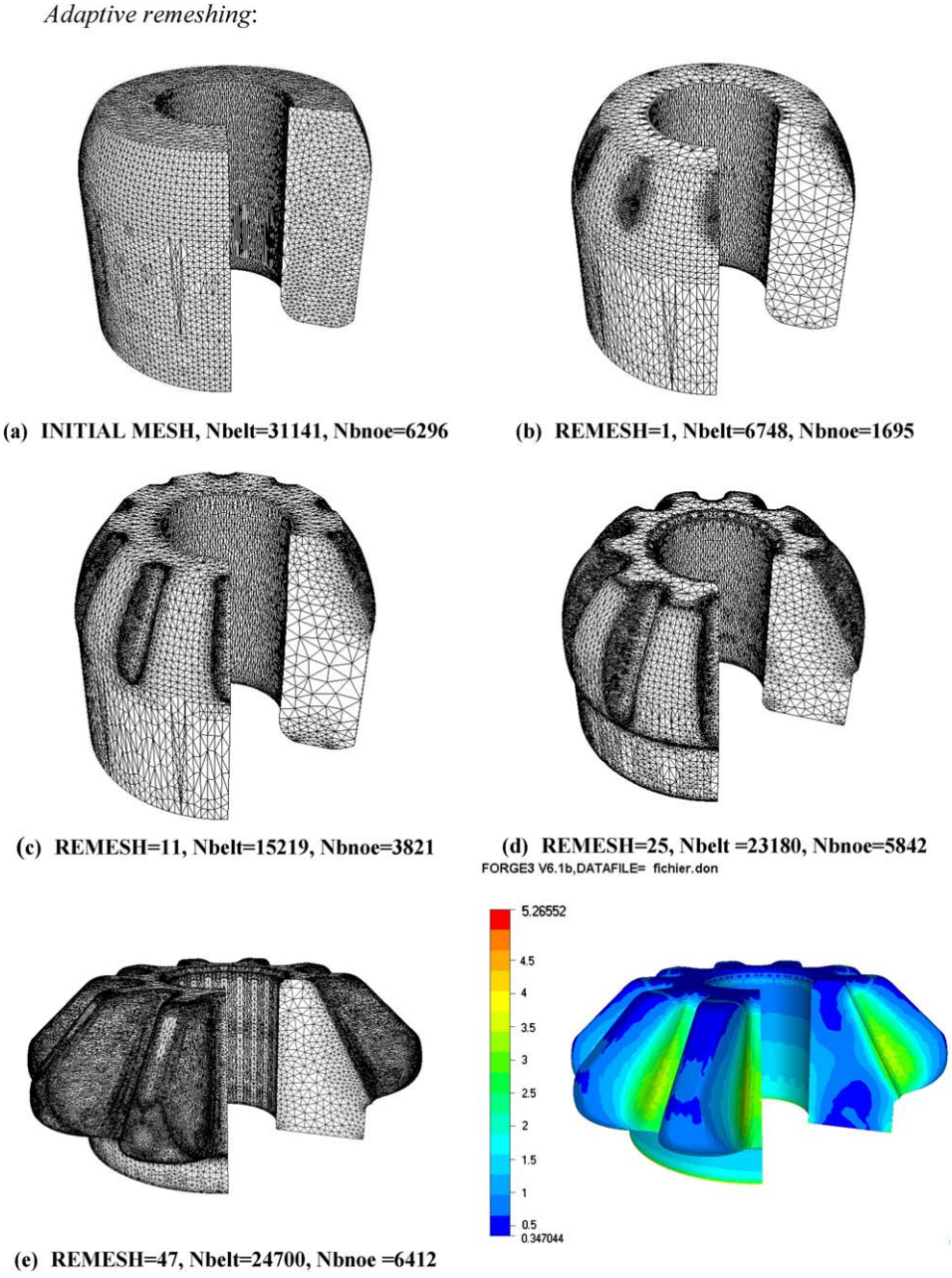

Fig. 19. Adaptive remeshing for the forging simulation of a gear and isovalues of the equivalent deformation.

$$\theta^{Z^2} = \|\tilde{e}_h\|_E = \left(\int_\Omega (\tilde{\sigma}_h - \sigma_h) : (\tilde{\varepsilon}_h - \varepsilon_h) \, \mathrm{d}\omega \right)^{1/2}, \tag{56}$$

where the recovery technique used to compute $\tilde{\sigma}_h$ is the same as for $\tilde{s}_h$ in the workpiece.

The elastic behaviour of the tools is defined by its Poisson ratio of $v = 0.3$ and its Young modulus of $E = 2 \times 10^5$ MPa. The imposed relative errors are 18% for the workpiece and 8% for the tools. The maximum number of admitted elements is respectively 20,000 and 15,000.

Figs. 16 and 17 show that same quality of results is obtained for the coupled problem, therefore allowing accurate calculations in the forging tools.

5.2. Gear forging

The forging of a gear is considered (see Fig. 18). The material follows the Norton–Hoff constitutive equation with: $m = 0.15$ and $K = 1.693 \times 10^3$ MPa. The initial part and dies temperatures are respectively 727 °C and 20 °C. The friction

law is viscoplastic (47) with: $\alpha = 0.3$ and $q = 1$. The imposed relative error is $\eta^{\text{imp}} = 10\%$ and the imposed maximum number of elements is $\text{Nbelt}^{\text{imp}} = 25{,}000$ (Figs. 19 and 20).

In order to analyse the interest of adaptive remeshing at a more practical level, the same simulation is carried out without adaptive remeshing based on error estimation. The mesh is refined only in some prescribed zones as shown in Fig. 21(a). Both simulations require approximately the same number of elements. From an engineering standpoint, the evolution of the forging force and numerical volume losses are compared in Figs. 22 and 23, respectively.

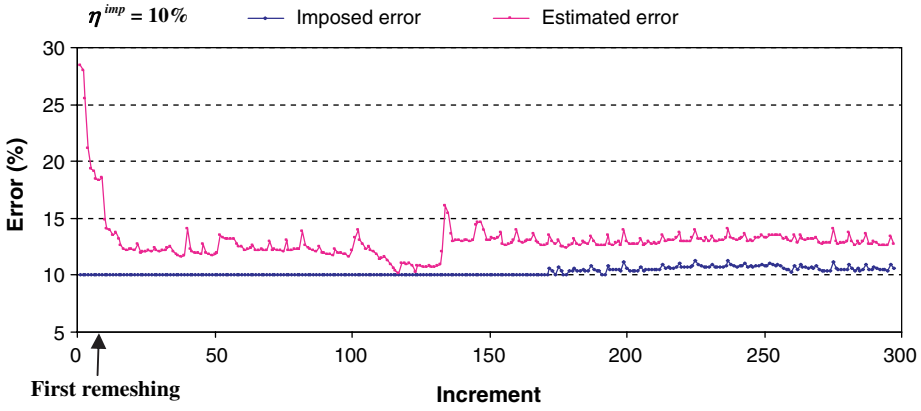

Fig. 20. Evolution of the estimated error during forging simulation of a gear.

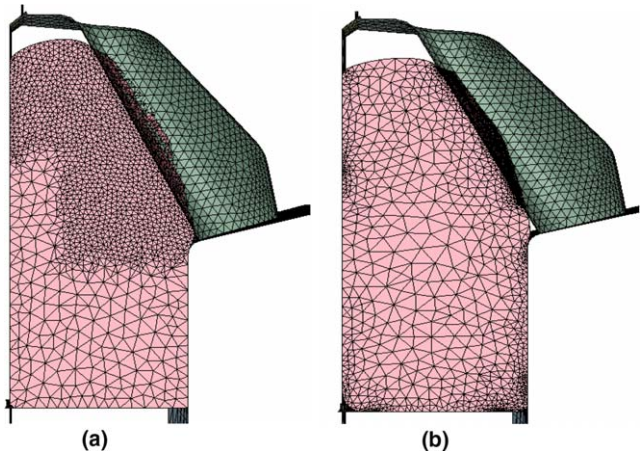

Fig. 21. Finite element meshes for the forging simulation of a gear. (a) Without user defined mesh adaptation. (b) With mesh adaptation based on error estimation.

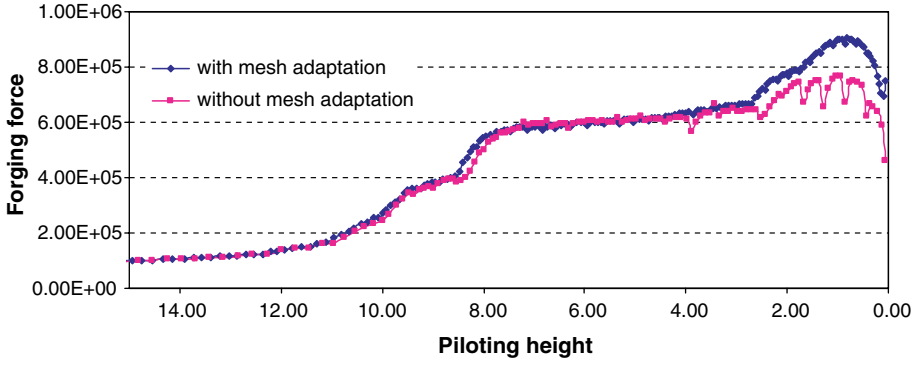

Fig. 22. Comparison between adaptive and "non-adaptive" finite element forging forces.

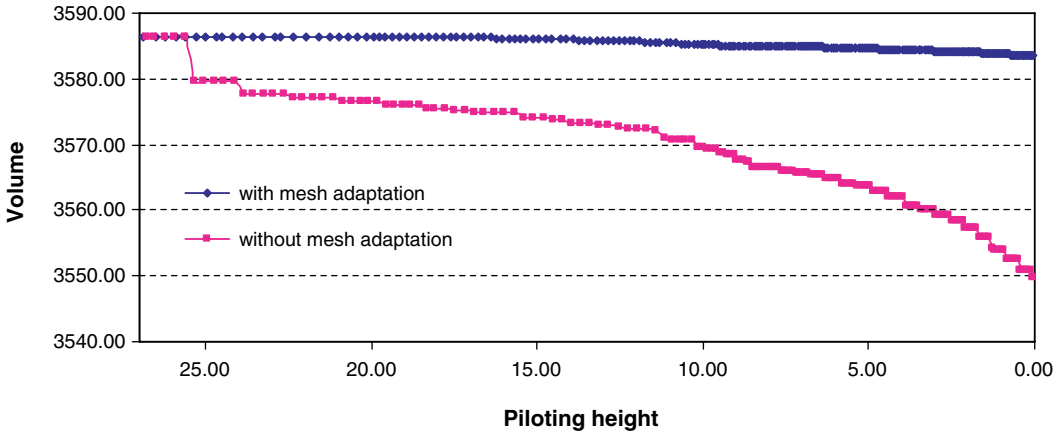

Fig. 23. Numerical volume losses for both simulations of gear forging.

Adaptive remeshing based on error estimation makes it possible to eliminate the numerical oscillations (see Fig. 22) due to coarse elements at the end of forging. Manually, it is very difficult to get rid of these oscillations by proper mesh refinement, due to the evolution of the flow. Optimal meshes also make it possible to dramatically reduce the numerical volume losses (see Fig. 23) also resulting from too coarse elements at the surface of the workpiece.

6. Conclusion

In 3D, for a velocity/pressure formulation and a viscoplastic constitutive law, the SPR procedure suggested by Zienkiewicz and Zhu produces enhanced stress fields that allow building a satisfactory error estimator. However, due to the inelastic behaviour of the material, superconvergence properties are not observed as in the elastic frame, and therefore the efficiency index of the estimation is less than 1. A correcting factor of 1.25 has to be introduced, as earlier noticed for 2D applications [12], to obtain a reliable error estimator.

The automatic 3D remeshing procedure, being based on an iterative mesh improvement by local changes, both for volume tetrahedra and surface triangles, makes it possible to continuously adapt the mesh size to a map provided by the error estimation procedure. The introduction of a constraint for the allowed maximal number of elements and of bounds for the refinement rate between successive remeshing steps provides a robust and reliable adaptive strategy for non-steady processes. 3D applications to forging simulations show this robustness, both with rigid and deformable tools. They also show the efficiency of the overall procedure, both from the scientific standpoint, as the finite element discretization error is controlled, and from engineer standpoint, as the best possible meshes are automatically produced, without requiring any finite element expertise, for prescribed computer resources. Practically, this approach allows reducing numerical instabilities (as for the forging force) and volume losses without increasing computational cost.

References

[1] T. Coupez, J.L. Chenot, Large deformations and automatic remeshing, in: E. Hinton, D.J.R. Owen, E. Onate (Eds.), Computational Plasticity (COMPLASIII), Pineridge Press, Swansea, 1992, pp. 1077–1088.
[2] T. Coupez, A mesh improvement method for 3d automatic remeshing, in: N.P. Weatherill et al. (Eds.), Numerical Grid Generation in Computational Fluid Dynamics and Related Fields, Pineridge Press, 1994, pp. 615–626.
[3] T. Coupez, S. Marie, R. Ducloux, Parallel 3d simulation of forming processes including parallel remeshing and reloading, in: Désidéri et al. (Eds.), Numer. Meth. Eng., ECCOMAS, Wiley & Sons, 1996, pp. 738–743.
[4] T. Coupez, L. Fourment, J.L. Chenot, Adaptive solutions in industrial forming process simulation, in: P. Ladeveze, J.T. Oden (Eds.), Advances in Adaptive Computational Methods in Mechanics, Cachan-Workshop, Elsevier, 1998, pp. 365–381.
[5] T. Coupez, Adaptive meshing for forming processes, in: M. Cross (Ed.), Numerical Grid Generation in Computational Field Simulation, U. of Greenwich, Mississippi State University, 1998.
[6] I. Babuška, W.C. Rheinboldt, A posteriori error estimates for the finite element method, Int. J. Numer. Methods Engrg. 12 (1978) 1597–1615.
[7] P. Ladevèze, G. Coffignal, J.P. Pelle, Accuracy of elastoplastic and dynamic analysis, in: I. Babuška, O.C. Zienkiewicz, J. Gago, E.R. de A. Oliveira (Eds.), Accuracy Estimates and Adaptive Refinements in Finite Element Computations, John Wiley & Sons Ltd., 1986, pp. 181–203 (Chapter 11).
[8] O.C. Zienkiewicz, J.Z. Zhu, The superconvergent patch recovery and a posteriori error estimates. Part II: Error estimates and adaptivity, Int. J. Numer. Methods Engrg. 33 (1992) 1365–1382.
[9] O.C. Zienkiewicz, J.Z. Zhu, A simple error estimator and adaptive procedure for practical engineering analysis, Int. J. Numer. Methods Engrg. 24 (1987) 337–357.
[10] O.C. Zienkiewicz, J.Z. Zhu, The superconvergent patch recovery and a posteriori error estimates. Part 1: The recovery technique, Int. J. Numer. Methods Engrg. 33 (1992) 1331–1364.

[11] M. Dyduch, Adaptive method in finite element simulations of metal forming processes, Ph.D. thesis, Faculté des sciences appliquées, Université de Liège, 1996.
[12] L. Fourment, J.-L. Chenot, Error estimators for viscoplastic materials: application to forming processes, Engrg. Comput. 12 (5) (1995) 469–490.
[13] T. Liszka, J. Orkisz, The finite difference method at arbitrary irregular grids and its application in applied mechanics, Comp. Struct. 11 (1980) 83–95.
[14] T. Coupez, S. Marie, From a direct solver to a parallel iterative solver in 3D forming simulation, Int. J. Supercomp. Appl. 11 (4) (1997) 205–211.
[15] T. Coupez, Génération de maillage et adaptation de maillage par optimisation locale, Rev. Eur. Élém. Finis 9 (4) (2000) 403–423.
[16] C. Gruau, T. Coupez, 3D tetrahedral, unstructured and anisotropic mesh generation with adaptation to natural and multidomain metric, Comput. Methods Appl. Mech. Engrg. 194 (48–49) (2005) 4951–4976.
[17] O.C. Zienkiewicz, Y.C. Lieu, G.C. Huang, Error estimates and convergence rates for various incompressible elements, Int. J. Numer. Methods Engrg. 28 (1989) 2191–2202.
[18] O.C. Zienkiewicz, J.Z. Zhu, The superconvergent patch recovery (SPR) and adaptive finite element refinement, Comput. Methods Appl. Mech. Engrg. 101 (1992) 207–224.
[19] P. Coorevits, E. Bellenger, Alternative mesh optimality criteria for h-adaptive finite element method, Finite Elem. Anal. Des. 40 (2004) 1195–1215.
[20] J. Barlow, Optimal stresses locations in finite element models, Int. J. Numer. Methods Engrg. 10 (1976) 243–251.
[21] I. Babuška, T. Strouboulis, C.S. Upadhyay, S.K. Gangaraj, Computer-based proof of the existence of superconvergence points in the finite element method; Superconvergence of the derivatives in finite element solutions of Laplace's, and the elasticity equations, Numer. Methods Partial Different. Equat. 12 (1996) 347–392.
[22] I. Babuška, T. Strouboulis, C.S. Upadhyay, S.K. Gangaraj, K. Copps, Validation of a posteriori error estimators by numerical approach, Int. J. Numer. Methods Engrg. 37 (1994) 1073–1123.
[23] O.C. Zienkiewicz, J.Z. Zhu, The superconvergent patch recovery and a posteriori error estimates. Part 1: The recovery technique, Int. J. Numer. Methods Engrg. 33 (1992) 1331–1364.